HIGH-LIFT-SYSTEM DESIGN FOR A LOW-NOISE MEDIUM-RANGE AIRCRAFT

F. N. Schmidt, D. Keller, M. Iwanizki, A. Seitz

German Aerospace Center (DLR), Institute of Aerodynamics and Flow Technologies,
Braunschweig 38108, Germany

Abstract

The DLR project "Low noise medium-range aircraft" (SIAM) has set itself the goal of designing an aircraft with the boundary conditions of "Flightpath 2050" in order to develop a significantly quieter configuration than modern conventional aircrafts with the most effective noise reduction technologies. Based on the work of Iwanizki et al.[3], the present paper describes the detailed design of a low-noise blended wing body with attached T-tail (hybrid wing body, HWB), which has considered the use of noise reduction technologies right from the start. As a basis for the wing design, the preliminary design and engine integration including the center body design are summarized. The final engine installation is a noise shielding effectively podded engine design at a streamwise position at 63 % of the center body length with an achieved drag reduction of ΔC_D = -0.0107 compared to the center body with unadapted integration. Based on the preliminary and the center body design, the wing geometry was built up with four section profiles. The profiles were designed using the inverse design capabilities of the DLR FLOWer code [22] realizing a local lift coefficient of c_l = 0.42 at Ma = 0.78 and a very limited supersonic region. Based on the cruise wing design, the high-lift configuration of the HWB with a gapless plain flap and an aileron was then realized, first with the help of 2D-RANS and afterwards 3D-RANS studies. Furthermore, a trailing edge flap with form adaptive shape was designed in order to realize a high-lift system without side edges reducing the noise emission of the wing further. The CFD investigations of the 3D high-lift configuration showed that the targeted lift coefficients of $C_{L,TO}$ = 0.76 and $C_{L,LDG}$ = 0.96 can be achieved by the HWB with the use of the designed conventional plain flap as well as with the morphing flap. The successful design of a gapless flap as high-lift system as well as the integration of the shielded engine are important steps of realizing a low-noise HWB regarding the goals of "Flightpath 2050".

1. INTRODUCTION

The "Flightpath 2050" by Europe's Advisory Council for Aviation Research and Innovation (ACARE) has set the ambitious goal of reducing the noise emissions of future aircrafts by 65 percent relative to typical new aircrafts from 2000.[1] Therefore, the DLR project "Low noise medium-range aircraft" (SIAM) has set itself the goal of designing an aircraft with the boundary conditions of "Flightpath 2050" in order to develop a significantly quieter configuration than modern conventional aircrafts with the most effective noise reduction technologies.

In the course of the SIAM project, Wienke et al. [2] compared several future low-noise aircraft configurations on pre-design level. The most promising design with regards to noise emission was a blended wing body design by Iwanizki et al. [3], which has the potential to reduce the perceived noise at all certification locations by more than 65 % compared to the 2000-era reference aircraft A320 with a conventional turbofan engine. The blended wing body configuration was developed by Iwanizki et al. within the SIAM project. The design consists of a blended wing body with attached T-tail and over the fuselage pylon mounted engines called hybrid wing body (HWB). The present paper describes the detailed design of the SIAM HWB with focus on the wing including the high-lift system design.

A blended wing body has already been presented as a future-oriented, low-consumption [4][5] and as a low-noise aircraft concept [6][7] in other international projects. The research question remains open how such a low-noise blended wing body and especially a low-noise high-lift system is designed in detail.

As Liebeck already stated, the advantage of a blended wing body is the great potential for noise reduction of the aircraft, in which the large area of the center body can be used for noise shielding effects.[8] Hileman et al. [9] also investigated a blended wing body as a low-noise aircraft and especially discussed the design of a low-noise high-lift system recommending to implement the wing as well as the low noise high-lift design right from the beginning of a low-noise aircraft design to reach the necessary high-lift performance as well as the low-noise requirements. In SIAM the goal of noise reduction was therefore incorporated into the aircraft design right from the start, which means that noise sources are reduced right from the beginning of the design process. Hence, low-noise concepts and their aerodynamic potential were consistently considered in the preliminary design as well as in the detailed design of the HWB. For the wing design implementing noise reduction right from the beginning means avoiding tracks, gaps or sharp side edges, as these are strong sources of noise emission especially during landing approaches as presented by Delfs [10] and Dobrzynski et al. [11]. The idea of the wing and high-lift design for the SIAM HWB is therefore to design a gapless high-lift system with the use of a plain flap. The detailed design of such a low noise wing including the low-noise flap system is described in more detail in the present paper. The presented detailed design of the HWB is based on the preliminary design by Iwanizki et al. and depends on the engine integration and center body design, which is why these design aspects are summarized first in the following sections.
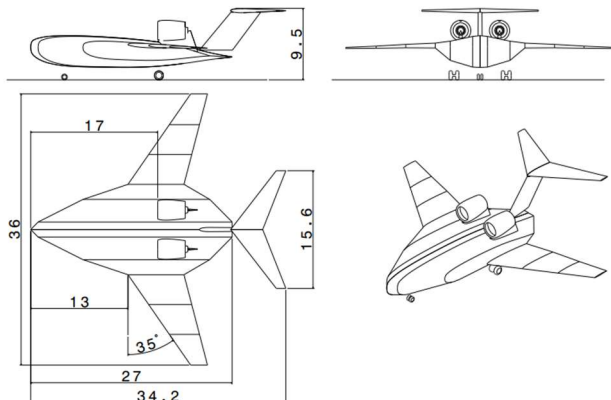
2. PRELIMINARY DESIGN

The great potential of the blended wing body for noise reduction is mainly resulting from the large area of the center body, which can be used for noise shielding effects as Liebeck [8] already stated. Furthermore, because of the additional lift of the fuselage and the integrated shape of the blended wing body the overall wetted surface of the aircraft concept can be reduced. Nowadays, the blended wing body is especially a design for bigger aircrafts (450 passengers). The goal of SIAM was to design a short to medium range aircraft for 180 passengers comparable to the reference aircraft A320.

Several challenges arise for a BWB of small size. One of them is the integration of a cabin with a feasible height in the aerodynamically shaped center body. Therefore, comparably thick airfoils are used in this section. As consequence, they provide a low maximum lift coefficient. The cabin is also located comparably far in the front of the center body leading to a large variation in center of gravity depending on the loading condition.

Focusing on the low noise emissions of the concept, the aircraft has been equipped with a low-noise gapless high lift system. Those devices provide a low contribution to the maximum lift. To achieve the low speed performance prescribed by the top-level aircraft requirements (TLARs) by a comparably low wing loading resulting in a large area of the aircraft.

In SIAM, the proposed aircraft had to provide sufficient handling qualities to remain operational by pilots without artificial augmentation and stabilization. This challenge was solved by the integration of a horizontal stabilizer to obtain a naturally stable aircraft at all loading conditions. A T-tail arrangement has been chosen as a most conservative approach. The tail also enabled the full utilization of the trailing edge flaps by compensating their pitch-down moment.

In order to exploit the full potential of the blended wing body concept for noise reduction, the engines have been installed above the center-body offering the shielding of the forward and rearward fan noise. The podded arrangement on pylons has been chosen to provide a separation between the nacelles and the center body and to increase the design freedom. The engine itself is an UHBR engine, which has a high potential to lowering the noise emission due to low exhaust jet velocities and reduced fan tip speeds.[12][13] The resulting pre-designed SIAM HWB is presented in Fig. 1 and the reference values of the aircraft are summarized in Tab. 1.

Fig. 1 Preliminary design of the "optimistic HWB" by Iwanizki et al. [3], which was defined as "SIAM HWB"

Tab. 1 Reference values of the SIAM HWB [3]

Parameter	Unit	Reference Value
Design range	[nm]	2600.00
Reference area	[m²]	348.10
Reference length	[m]	5.35
Design Mach number Cruise	[-]	0.78
Mach number LDG	[-]	0.20
Mach number TO	[-]	0.23
Total lift coefficient at Cruise (pre-design)	[-]	0.23
Maximum lift coefficient TO (pre-design)	[-]	0.76
Maximum lift coefficient LDG (pre-design)	[-]	0.96
Lift-to-Drag-Ratio, rel. deviation w.r.t. SIAM tube-and-wing baseline (pre-design)	[-]	-3%
Fuel consumption, rel. deviation w.r.t. SIAM tube-and-wing baseline (pre-design)	[-]	+3%

Comparing the SIAM HWB by Iwanizki et al. to other designs it has to be stated that the name "HWB" is originally based on the aircraft design by Hooker et al. [4]. Hooker et al. designed a HWB-based freighter with technology levels from 2030-2035 resulting in up to 7 % less fuel consumption than an advanced tube-and-wing configuration using the same technology levels.[14][15][16] Hereby, Hooker et al. designed different variations of a HWB with reference to a Boeing 757 and a Boeing 777. Their design HWB 757 for a range of 2450nm had a final cruise lift-to-drag-ratio of L/D=19.8 at a cruise Mach number of Ma=0.81.[15] Comparable to the HWB of Iwanizki et al. the design by Hooker et al. has over the fuselage pylon mounted engines and a T-tail. Hooker et al. designed the engine's position of the HWB close to the trailing edge of the wing. The position of the pylon mounted engine close to the trailing edge of the aircraft also corresponds to the results from an additional study by Hooker et al. [17], when designing an over the wing nacelle for improved energy efficiency. The best position of the nacelle was close to the trailing edge of the wing according to the aircraft's total drag and therefore it's fuel efficiency. However, if the aircraft design is primarily driven by the goal of reducing noise, the engine must be installed further forward in order to take full advantage of the shielding effect regarding the engine noise, which leads to a significantly greater challenge when integrating the engine above the center body.

3. ENGINE INTEGRATION AND CENTER BODY DESIGN

Due to the requirements with regards to noise shielding and natural stability/handling qualities, the streamwise engine position is fixed at 63 % of the center body length. From an aerodynamic perspective, the location poses significant installation challenges. Fig. 2 shows the flow field in terms of Mach number and the surface pressure distribution of the center body at the engine's center line section. The black line thereby represents the C_p distribution without engine and the red line the one with engine. The figure reveals a deceleration of the flow ahead of the nacelle. At the position of the nacelle lip the flow begins to accelerate due to the channel effect. Further downstream, the flow within the

channel between the center body and the nacelle experiences a shock, causing a sudden increase in the surface pressure. Towards the trailing edge, the flow then decelerates further while the stagnation pressure at the trailing edge does not reach the one found for the case without engine. As a result, the drag in cruise flight substantially increases by ΔC_D=0.0111 (83%) compared to the combination of the isolated wing-body and isolated nacelle. The problem with the engine integration over the center body of a BWB and the risks of the indicated local flow acceleration between the nacelle and the center body are already known from studies e.g. by Xin et al [18]. Xin et al. were able to mitigate the channel effect and significantly reduce the strong shock waves by optimizing the shape of the channel between the engine and the fuselage of the BWB with the help of 3D RANS studies.
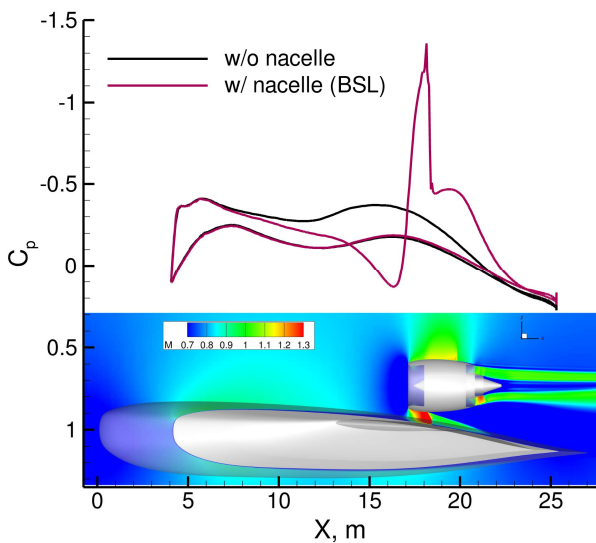

Fig. 2   Flow field and surface pressure distribution of center-body at engine's center section

In order to reduce the installation drag of the SIAM HWB, the engine integration was therefore modified based on the following approach.

- In a first step, a sensitivity study was carried out to assess the impact of the vertical and streamwise engine position, the engine incidence angle, and the freestream Mach number.
- In parallel, the nacelle was designed for cruise flight conditions with 2D and 3D RANS computations. Low speed off-design conditions were thereby considered as well.
- Then, the 2D section at the engine's center line was parameterized and optimized via 2D-RANS computations. Since the representative 2D geometry includes the highly swept center-body and the nacelle, considerable effort was dedicated to find reasonable 2D boundary conditions. Two approaches have been followed, here. In the first approach, only the upper rear part of the center-body section and the nacelle were modified ("local modification"). The cabin dimension has not been considered in the first approach. In the second approach, the entire center-body section was modified while the cabin dimensions were considered as geometric constraint.

- Based on the results of the 2D-RANS optimizations, the parameterized 3D CAD model was adapted. The model was then modified in spanwise direction with the help of 3D-RANS computations.
- In parallel to the spanwise modifications, the engine pylon was designed and integrated.

Fig. 3 compares the initial geometric shape (black line) with the resulting ones from the 2D optimization for the "local modification" approach (green line) and the "entire section" approach (red line). While the upper rear part of the center body and the engine shape of the two optimized shapes look very similar to each other, the front and mid part of the second approach is notably thicker as the optimizer has to consider the shape constraints from the cabin.
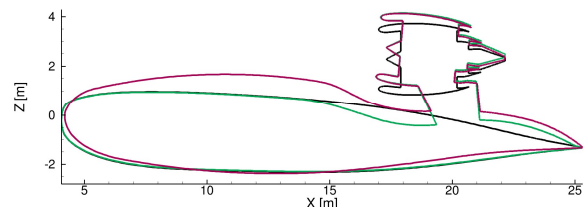
Fig. 3   Geometric shape at engine's center section before (black line) and after optimization (green line: local modification and red line: entire center-body section)

Fig. 4 compares the resulting surface pressure distributions of the "local modification" approach to the initial one after the transfer of the optimization results to the 3D model and the subsequent additional spanwise modifications. The comparison of the surface pressure distribution indicates that the deceleration ahead of the nacelle, which is accompanied by higher pressure, the acceleration between the nacelle and the center body, and the shock downstream, which are all visible on the initial shape, vanish due to the modifications.
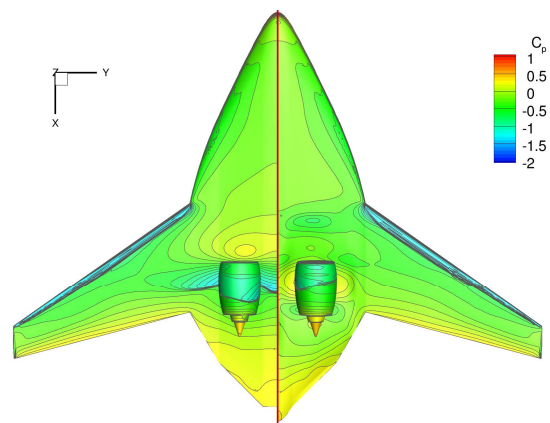
Fig. 4   Comparison of surface pressure distribution on the upper side at cruise conditions. Left: Initial shape, right: Local modification

A final drag penalty assessment (including changes in net thrust) finds a change of ΔC_D = 0.0004 (+3.0%) for the first approach compared to the combination of the isolated airframe in conjunction with the isolated engine. In contrast to the optimized shape, the isolated case does not include a pylon. Excluding pylon forces of the optimized shape, the

change in drag/net thrust is ΔC_D = -0.0002 (-1.5%). Compared to the initial shape, the optimized shape yields an improvement of ΔC_D = -0.0107. In the case of the second approach the improvement compared to the initial shape is less with ΔC_D = -0.0099. Compared to the isolated case, the drag penalty is ΔC_D = 0.0012 (9.0%, including pylon forces). More information on the engine integration can be found in [19].

4. WING DESIGN

In the following section, the design of the clean wing, i.e. the HWB in cruise configuration, and the wing with the extended high-lift system are presented. The design of the wing in cruise and in high-lift configuration was carried out in several parallel iterations, since parameters such as the twist distribution or the relatively thickness of the wing profiles influence the aerodynamic performance of both configurations.

4.1. Cruise Wing Design

Starting point of the cruise wing design were the results of a preliminary overall aircraft design as pointed out in section 2 and shown in Fig. 1. This "optimistic HWB" configuration was subsequently frozen, so the basic dimensions of the wing, i.e. span, area, taper and sweep angle were fixed.
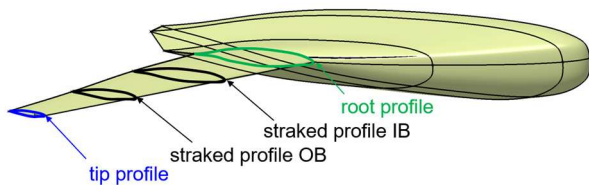

Fig. 5 Simplified HWB with the cruise wing consisting of a wing root profile (green), a wing tip profile (blue) and two straked middle profiles (bold black)

The detailed wing design consisted essentially of the specification of two generator wing sections (or profiles, respectively) located at wing root and wing tip with two more sections straked linearly in-between (see Fig. 5) according to the following requirements:

- The design point is given by a cruise Mach number of M = 0.78, with a total lift coefficient of $C_{L, tot}$ = 0.23 at flight level FL380, which translates into an altitude of H = 11582m. The corresponding Reynolds numbers at root and tip are Re_{Root} = 40.04 million and Re_{Tip} = 12.27 million, respectively.
- The boundary layer flow about the wing is full chord turbulent.
- The required local lift coefficient at $C_{L,tot}$ is approximately c_l = 0.42, see the spanwise distribution of local lift coefficients in Fig. 6 from the preliminary design step.
- A spanwise thickness distribution was not specified in the preliminary design phase. Instead, a profile adapted from the profiles of the VELA blended wing body [20] with 6% relative thickness was used as generator section for the wing. However, a first aerodynamic analysis of this configuration with RANS simulations using the high-fidelity flow solver DLR Tau [21] at Ma=0.78 and cruising altitude revealed that at the design lift coefficient a strong suction peak with minimum C_P of -1.5 followed by a very strong compression shock is present over the inboard wing at

around 15% chord (see Fig. 7). Design goal then was to remove this suction peak by utilizing the design principles for modern transonic, swept wing profiles. Additionally, in order to keep the wing mass low, relative thickness should be as high as possible without compromising low wave drag properties.
- The twist has to be adjusted as a good compromise between spanwise lift distribution at design point (induced drag) and high-lift requirements (local $c_{l,max}$ on outboard wing, see section 4.2).
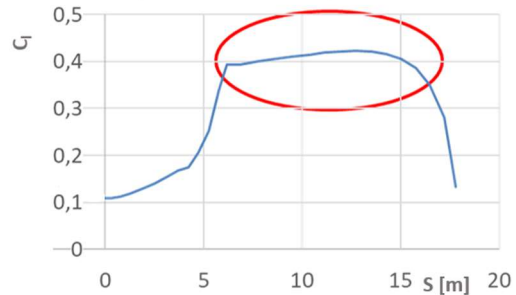
Fig. 6 Spanwise distribution of local lift coefficient c_l
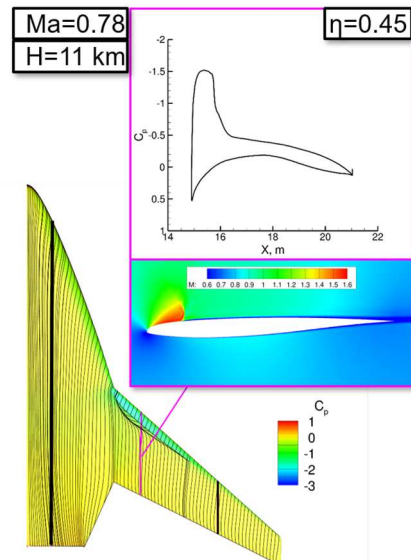
Fig. 7 Surface streamlines in combination with the pressure coefficient and the flow field at η=0.45 of the pre-designed wing at design lift coefficient

Using the inverse design capabilities of the DLR FLOWer code [22], a finite volume RANS solver on structured grids, for the root generator section a target pressure distribution (see Fig. 8) was defined with the following features:

1. The pressure distribution delivers c_l = 0.42 at Ma = 0.78. It is valid for an infinitely swept wing with a sweep angle of ϕ = 25°. This value corresponds to the local sweep at chord position 50% for the swept and tapered wing.
2. The supersonic region is very limited (C_{P}^{*}, crit denotes the pressure coefficient at which the Mach number based on the velocity normal to the isobars exceeds the speed of sound) with a maximum local Mach number of 1.06 on the suction side of the profile. As a consequence, recompression is almost shock free with a wave drag below 1 drag count, while viscous and form drag come to a total of c_d = 0.00672 at a mean Reynolds number of 25 million. Furthermore, the

pressure rise over the rear part of the profile has a concave shape on the upper as well as the lower side, which contributes to the low total drag, see Eppler [23].

3. In order to keep the zero-lift pitching moment low, the pressure distribution exhibits a strong front and a low rear loading. Consequently, c_{m25} is only 0.00978.
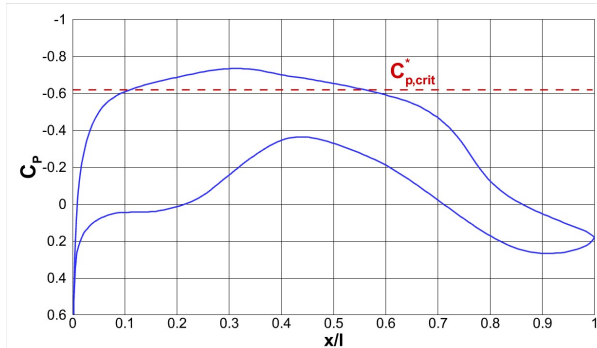

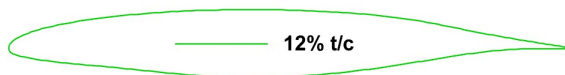**Fig. 8 Target CP distribution for root generator profile**

Fig. 9 Contour of 12% thick root generator profile

The resulting profile shape with 12% relative thickness is shown in Fig. 9. From this contour, the tip generator section was derived, which shows essentially the same features except a 13% larger nose radius for improved low speed characteristics.

4.2. High-Lift-System Design

On the basis of the preliminary design, the center body design and the cruise wing design the high-lift system of the SIAM HWB was developed. Since the HWB including its reference area were dimensioned in the preliminary design with the boundary condition of a low-noise wing, the high-lift system of the HWB consists of a gapless plain flap mainly used for lift increase during take-off and landing as well as an aileron for flight control around the longitudinal axis. Two variants of the flap were designed for the HWB: Variant 1 ("plain flap") is a conventional gapless plain flap, which still has side edges as source of noise emission.[10] The flap side edge noise can be significantly reduced by means of porous edge treatments, as Fink et al. [24] as well as Dobrzynski et al. [11] have already demonstrated. Variant 2 ("morphing flap") is a gapless plain flap designed with form adaptive side edges comparable to the design by Kota et al. [25] as well as the adaptive trailing edge developed by the TU Munich within the BMWi project "FlexMat" in co-operation with the DLR [26]. Hereby, the gapless flap is designed as a trailing edge flap with variable shape in order to further reduce the noise emissions of the high-lift configuration in comparison to the "plain flap" with side edges.

The boundary conditions of the flap design are generating enough lift during take-off and landing with a limited impact on the moment balance in terms of flight stability at the same time.[27] Another boundary condition to be realized is the maximum lift coefficient during take-off $C_{L,max,TO}$=0.76 and landing $C_{L,max,LDG}$=0.96 that were approximated by the preliminary design.

For a first estimate of $C_{L,max}$ 2D simulations were carried out

with the first design of the clean wing profiles as well as flap deflection studies for the designed wing profiles. Based on the results of the 2D studies, a design process chain was set up for the 3D high-lift design of the HWB with both flap variants.

4.2.1. 2D Design Studies

The starting point of the 2D design studies of the flap was the straked profile OB (see Fig. 5) as it is located at the section with the highest loading of the wing considering Fig. 6. The studies were initially carried out primarily for the landing configuration, because it requires the highest total lift coefficient $C_{L,max,LDG}$=0.96. The procedure for designing the take-off configuration was fulfilled similar.

As described in section 4.1 the HWB should have a total lift coefficient of $C_{L,tot} = 0.23$ in cruise conditions with a required local lift coefficient of approximately $c_{l,loc} = 0.42$. Since the 2D studies were performed with the use of the profile perpendicular to the leading edge the wing's sweep needs to be considered as well with $\phi_{25} = 30.58°$. Considering the ratio between the required local lift coefficient of the wing section in relation to the total lift coefficient as well as the swept wing with

$$c_{l,2D,LDG} = C_{L,max,LDG} \cdot \frac{c_{l,loc}}{C_{L,tot}} \cdot \frac{1}{\cos(\phi_{25})^2}$$

the necessary lift coefficient for landing is resulting to $c_{l,2D,LDG} = 2.38$.

The Mach number for the flap design was specified by the preliminary design with $Ma_{LDG} = 0.2$, which results in an effective Mach number for the 2D perpendicular profile of $Ma_{eff,LDG} = 0.1722$. For the design of the flap, the maximum possible relatively flap chord length of 25 % was assumed, which was predefined based on the spar position of the preliminary design.

First, the clean profile was analyzed using fully turbulent 2D-RANS simulations with the flow solver DLR Tau for different angles of attack. The trailing edge of the wing profile was then modeled at $x/c = 0.75$ with different deflection angles δ and simulated in each case with the same boundary conditions as for the clean profile. The resulting lift and drag coefficients are presented in Fig. 10.

The results for the different force coefficients are consistent with comparable studies such as Spearman's wind tunnel tests on the NACA 0009 Airfoil with a 0.25-airfoil-chord plain flap.[28] The deflected plain flap increases the profile camber of the profile and due to the associated change in the Kutta condition and the resulting change in the airfoil's circulation the lift coefficient is increased at the same angle of attack with increased flap deflection angle. At the same time the angle of attack of $c_{l,max}$ decreases as the flap deflection angle increases.

The increase in the lift coefficient with the deflection angle does not increase linearly, but becomes smaller as the deflection angle increases further. In addition, the lift coefficient curve is almost linear in the low angle of attack range up to a flap deflection angle of $\delta = 10$ deg, whereas for the cases with a flap deflection angle of $\delta = 15$ deg and $\delta = 20$ deg the lift suddenly changes at smaller AoA.
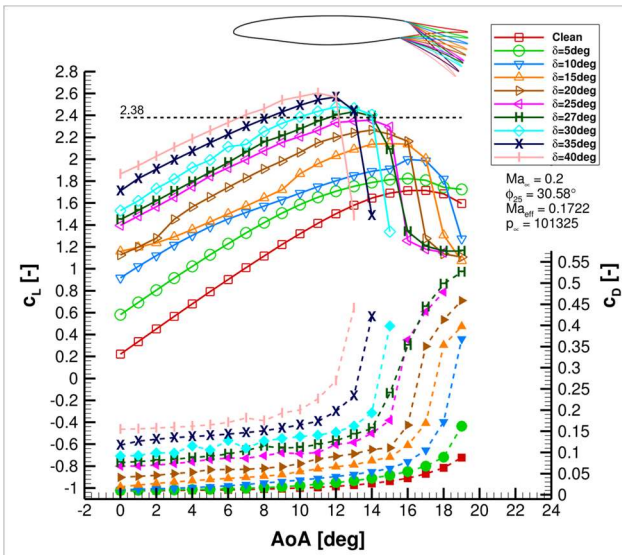
Fig. 10 Lift and drag coefficients over angle of attack for the clean wing section profile and the section profile with different trailing edge deflection angles

As it can be seen in Fig. 11, the flow at the plain flap begins to detach at an angle of attack of AoA=0 deg and a deflection angle of δ = 15 deg. This detachment in the trailing edge region of the plain flap expands further forward as the deflection angle is further increased to δ = 20 deg until the flap is completely detached at a deflection angle of δ = 30 deg. Due to the flap kink, however, there is still an increase of the lift coefficient even when the flap is detached. Even if the angle of attack is further increased, the separation remains locally on the flap and does not expand further forward onto the main profile.
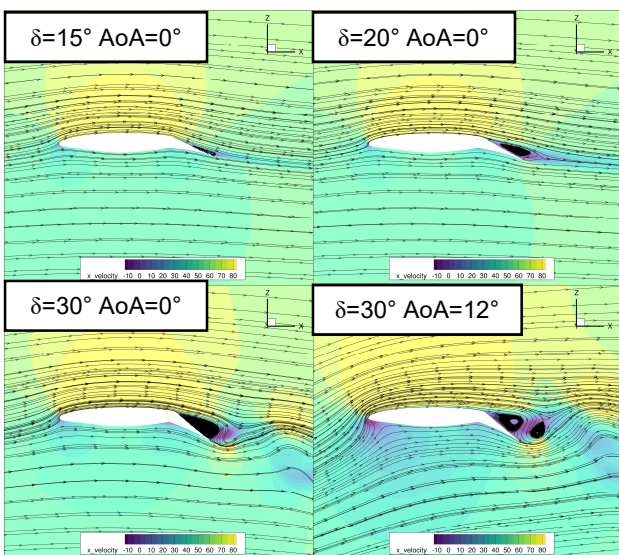
Fig. 11 Flow field including velocity streamlines of the 2D plain flap for different deflection angles

In addition, the most important result of the 2D investigations is that the previously estimated lift coefficient $c_{l,2D,LDG}$ = 2.38 can be achieved at a deflection angle of δ = 27 deg. The flap is already partially detached for the deflection angle of δ = 27 deg, which has positive effects to generate additional drag during landing.

4.2.2. 3D Design Studies

On the basis of the results of the 2D design studies, the 3D design of the flap in landing configuration begun with a deflection angle of δ = 27 deg as the starting point. Considering the specifications of the preliminary design the goal of the 3D design was to realize a total lift coefficient of $C_{L,LDG}$=0.96 only with the components of the center body and the wing including the deflected flap. Added later are the engine and T-tail, which also make a positive contribution to the lift coefficient and thus offer additional security for the lift generation.

The flap design was initially carried out for the conventional plain flap. The procedure was then transferred to the design of a morphing flap. All 3D studies on the high-lift system were carried out with the DLR Tau flow solver using RANS simulations. The simulations were carried out using the SA-RC single-equation turbulence model with a central dissipation scheme with matrix dissipation. The boundary layers close to the wall were being assumed to be fully turbulent.

4.2.2.1. Plain Flap

For an initial assumption, the flap system of the HWB was divided into three equally wide sections. The IB flap initially goes from the wing root profile to the straked profile IB and the OB flap is located between the two straked wing profiles (see Fig. 5). For the design of the HWB's high-lift system, a CAD model with a parametric inboard and outboard trailing edge flap was set up. The resulting baseline geometry of the HWB with the plain flaps initially deflected by δ = 27 deg can be seen in Fig. 12.
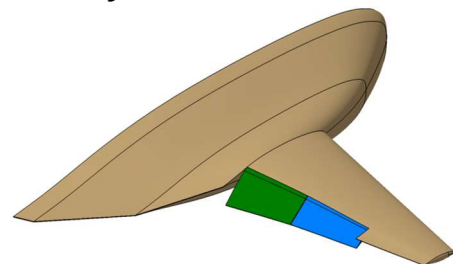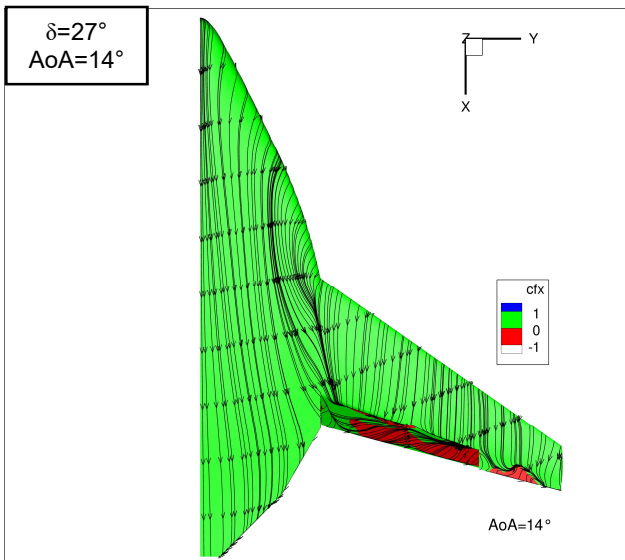

Fig. 12 Simplified HWB for the 3D high-lift studies with the IB flap (green) and the OB flap (blue) both deflected by δ = 27 deg

The resulting force coefficients of the RANS simulations with the simplified HWB including the center body, wing and the plain flap with δ = 27 deg can be seen in Fig. 13.

Looking at the lift coefficient of the simplified HWB, it becomes clear that with a flap deflection of δ = 27 deg, the target lift coefficient of $C_{L,LDG}$ = 0.96 is reached at an angle of attack of AoA = 14 and therefore just before AoA($C_{L,max}$). Hence, the previously simplified assumptions and 2D studies carried out provide a very good basis for the first draft of the plain flap.
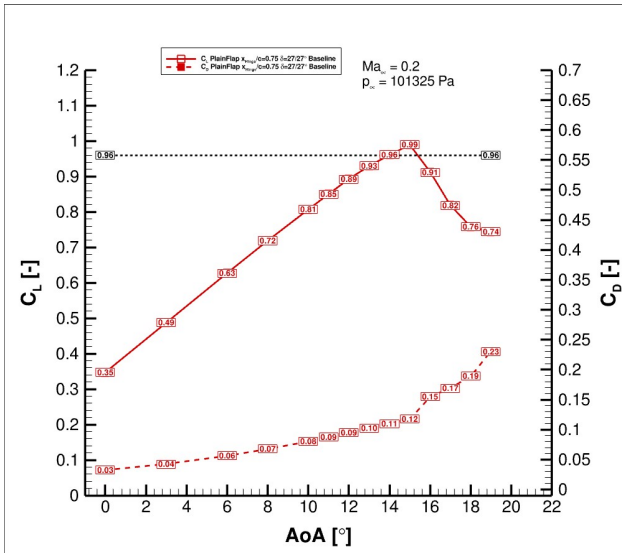
Fig. 13 Lift and drag coefficients over angle of attack for the simplified HWB baseline with δ = 27 deg

However, upon closer inspection of the surface solution of this design in Fig. 14 it is obvious that when the desired lift coefficient is reached at AoA = 14deg, the flow begins to separate in the outboard region of the wing.


Fig. 14 Surface streamlines and plotted skin friction of the simplified HWB baseline with δ = 27 deg

The region of the separated flow on the outboard wing is close to the trailing edge where the aileron is located. However, if an undeflected aileron is already largely separated, the stability/handling of the aircraft cannot be guaranteed considering the aircraft's certification since the HWB needs to be controlled even in the near-stall region. Therefore, as described in section 4.1, the profile in the tip section was thickened and a profile with an increased nose radius was used to weaken the pressure's suction peak and thus reduce the risk of detachment in the tip region. In addition, the twist was adjusted as a good compromise between spanwise lift distribution at cruise design point and the local $c_{l,max}$ of the high-lift configuration. The final twist of the wing can be seen in Tab. 2.

**Tab. 2 Optimized vs. preliminary designed twist distribution of the HWB's center body and wing**

	Loc. twist (optimized)	Loc. twist (baseline)
Section 1 (body)	0,0°	0,0°
Section 2 (body)	0,0°	0,0°
Section 3 (body)	1,0°	1,0°
Section 4 (root profile)	-1,21°	0,247°
Section 4a (straked profile IB)	-1,672°	-1,055°
Section 4b (straked profile OB)	-1,364°	-0,801°
Section 5 (tip profile)	-5,969°	-2,411°

The resulting reduced twist in the outboard region of the wing in combination with the increased nose radius of the tip section profile leads to a new wing geometry, which was investigated again with the use of RANS flow simulations. Due to the changed twist and section profile, the deflection angle of the updated wing had to be increased up to δ = 30 deg to realize nearly the same total lift coefficient compared to the baseline as presented in Fig. 15. With the optimized wing geometry and an deflection angle of δ = 30 deg the necessary total lift coefficient of $C_{L,LDG}$ = 0.96 is again reached at the angle of attack of AoA = 14.
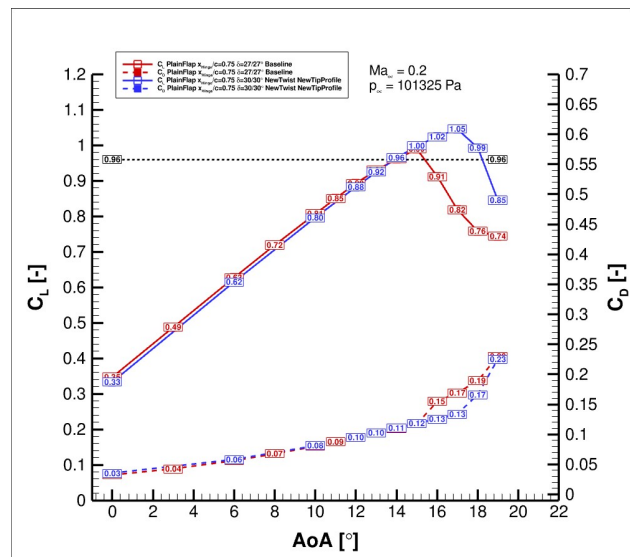

Fig. 15 Lift and drag coefficients over angle of attack for the simplified HWB baseline with δ = 27 deg (red) and the optimized wing with δ = 30 deg (blue)

In addition, the optimization of the wing geometry successfully leads to a stall delay about 2 deg compared to the baseline. The improvement of the wing in terms of flow separation can also be seen, when analyzing the surface streamlines presented in Fig. 16. In the tip region of the optimized wing, the flow is now almost completely attached at an angle of attack of AoA = 14 deg, which improves the handling of the HWB reaching $C_{L,LDG}$ = 0.96.
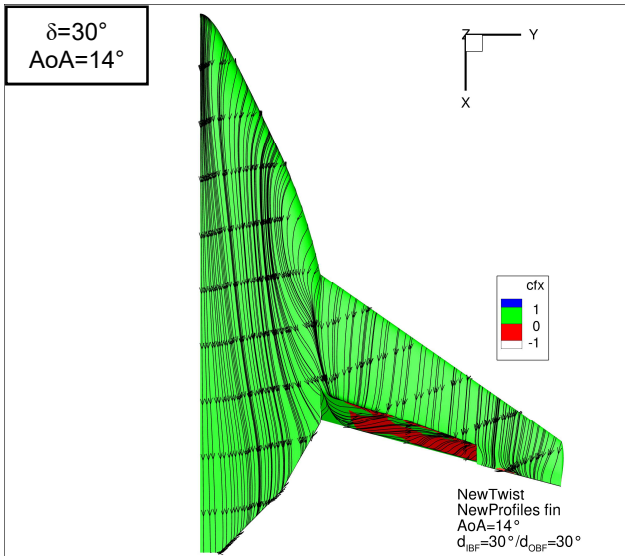
Fig. 16 Surface streamlines and plotted skin friction of the optimized HWB wing geometry with δ = 30 deg

Finally, the designed wing geometry with the optimized plain flap was combined with the design from the parallel progressing engine integration. As already described in section 3, the rear shape of the center body in particular has been optimized in order to reduce the installation drag of the SIAM HWB. In Fig. 17 the final plain flap geometry is combined with the original center body geometry that was used during the flap design studies and with the optimized center body geometry. In addition, the entire center body and wing geometry was rotated by 3 degrees during the engine integration.
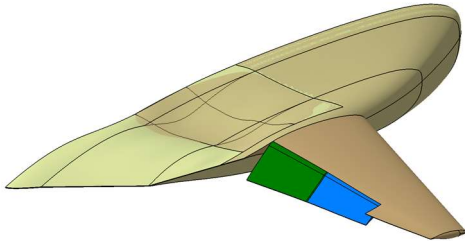
Fig. 17 Final plain flap geometry with δ = 30 deg in combination with the original as well as with the engine optimized center body
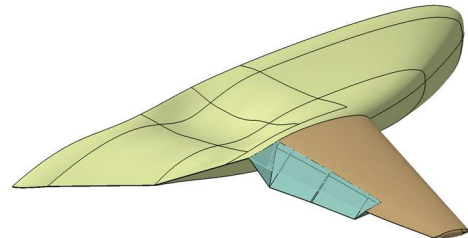
The resulting force coefficients for the final geometry are shown in Fig. 18. As it can be seen, the optimized shape of the center body has only a small influence on the lift coefficient in the low-speed. Only the rotation of the center body and wing is clearly visible, in that the entire lift curve is shifted by 3 deg due to the changed local angle of attack. With this final wing geometry, the desired lift coefficient of $C_{L,LDG}$ = 0.96 is achieved at an angle of attack of AoA = 11 deg.
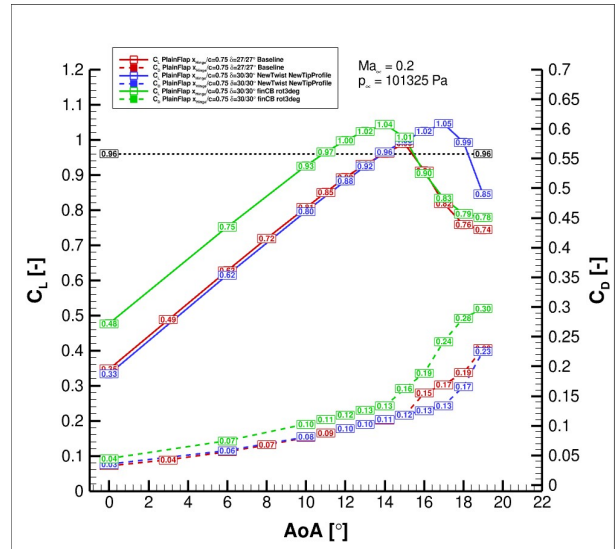
Fig. 18 Lift and drag coefficients over angle of attack for the baseline with δ = 27 deg (red), the optimized wing with δ = 30 deg (blue) and the final wing with δ = 30 deg with the final center body (green)

4.2.2.2. Morphing Flap

The procedure for designing the plain flap with form-adaptive sides was equivalent to the design of the conventional plain flap, which is why this section focuses primarily on the differences and special features of the design. The morphing flap is based on the experiences of Radestock et al. [29] collected during the BMWi FlexMat project, in which a demonstrator model of a plain flap with variable shape side edges has been successfully built up.

In particular the shape adaptive side edges of the flaps can be realized by a shape adaptive gap cover triangle based on a hybrid matrix fiber composite material concept. The gap cover triangle consists of hinges connected to the main wing as well as to the flap, a 3D printed core and a covering skin. [29] The idea of the gap cover triangle is to use a combination of hard and soft material with the result that the gap cover itself can resist the aerodynamic forces acting on it, but is also flexible enough to adapt its form, when the plain flap is deflected. In Fig. 19 the final morphing flap geometry is presented in landing configuration with δ = 33 deg and in addition in take-off configuration to visualize the nearly retracted flap with δ = 3 deg.


Fig. 19 Final morphing flap geometry with δ = 3 deg and δ = 33 deg in combination with the engine optimized center body

The resulting force coefficients of the HWB with morphing flap can be seen in Fig. 20 in comparison to the force coefficients of the designed plain flap. Finally, the results for the take-off configuration of the two variants are presented as well in Fig. 20, which were designed with a similar design procedure as the landing configuration. It should be noted

that regarding the preliminary design the landing configuration was designed for Ma=0.2, whereas the take-off configurations were designed at Ma=0.23.
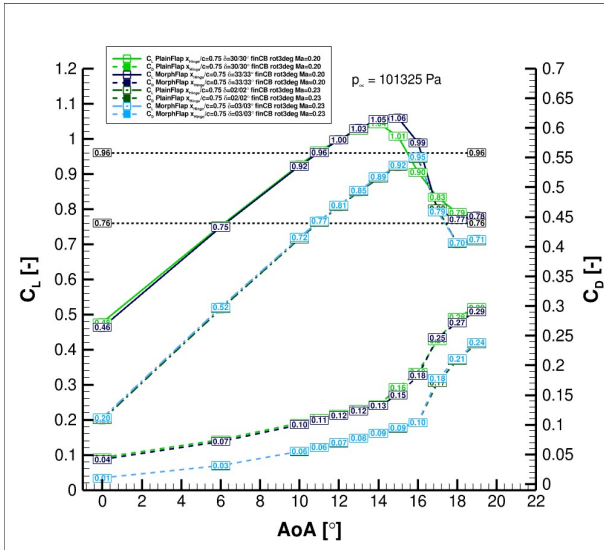

Fig. 20 Lift and drag coefficients over angle of attack for the final HWB wing with plain and morphing flap in landing and take-off configuration

The results of the final CFD investigations of the 3D high-lift wing configuration demonstrate that the lift coefficient of $C_{L,TO} = 0.76$ and $C_{L,LDG} = 0.96$ can be achieved by the HWB with the use of the designed conventional plain flap as well as with the morphing flap. Despite the stall behavior the values for the lift and drag coefficient are nearly the same comparing the two variants.

4.2.2.3. Aileron

Since the target lift coefficient of $C_{L,LDG} = 0.96$ can be achieved with both the plain flap as well as the morphing flap, an additional aileron deflection to increase the lift coefficient of the wing during landing is not intended. Nevertheless, the effectiveness of the aileron must be ensured over the entire angle of attack range. Hence, the aileron is sized as wide as possible expanding nearly over the whole outer wing. The hinge line of the aileron was defined by the spar and is positioned at $x/c_{wing}=0.75$. The resulting geometry of the aileron can be seen in Fig. 21 for the plain as well as the morphing flap configuration.
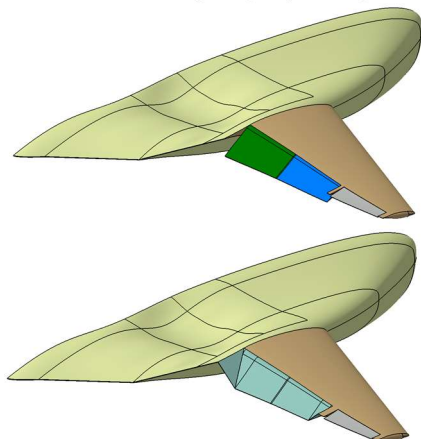
Fig. 21 Plain flap (top) and morphing flap configuration (bottom) with deflected aileron with $\delta_{Aileron}$ = 5 deg

Due to structural constraints, the width of the main wing bridge between the aileron and the morphing flap is greater than the width for the plain flap variant, since components as the hinges need to be installed between the main wing and the morphing flap. As it can be seen in Fig. 22, the flow at the aileron is fully attached at a deflection angle of $\delta_{Aileron}$ = 5 deg in both variants for AoA = 0deg. For AoA = 11deg the flow at the aileron begins to detach in both cases, but the aileron is dimensioned large enough to have an attached flow in the outboard region to ensure rolling stability of the aircraft.
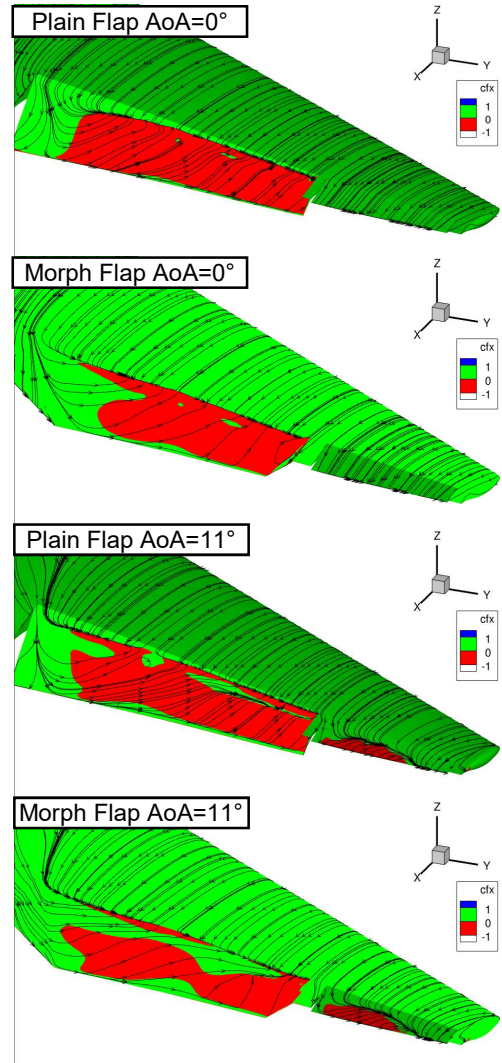
Fig. 22 Surface streamlines and plotted skin friction of the plain flap and the morphing flap with deflected aileron $\delta_{Aileron}$ = 5 deg

5. FIRST PERFORMANCE EVALUATION OF THE LANDING AND TAKE-OFF CONFIGURATION

For an initial analysis of the designed configurations, full thrust at Ma=0.23 for the take-off configuration and idle thrust at Ma=0.20 were simulated for the HWB's podded engine. The simulations were carried out for both variants of the designed flap system with the final HWB with T-tail and optimized center body. First results of the investigation of the final HWB in high-lift configuration are shown for the angle of attack AoA = 0deg in Fig. 23.
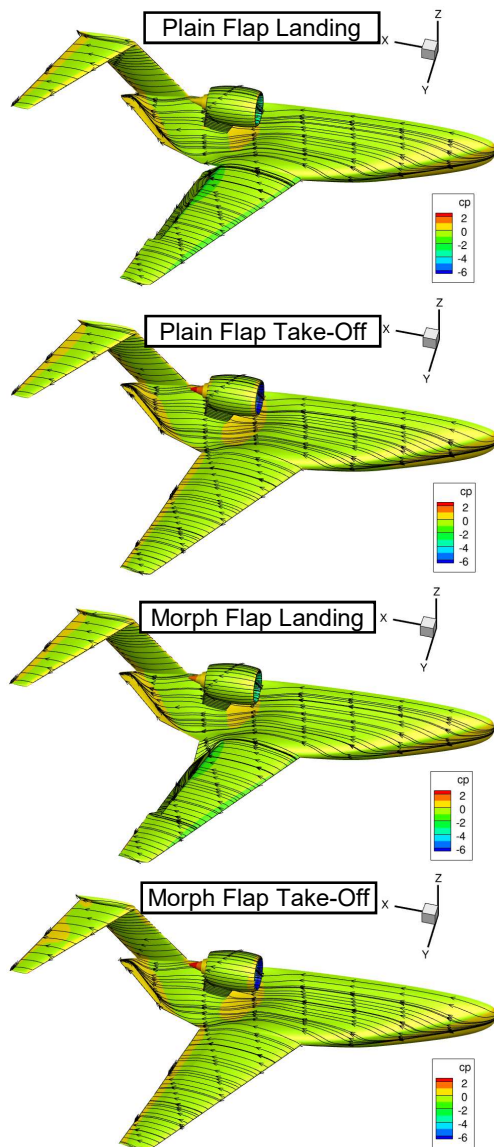
Fig. 23 Surface streamlines and pressure coefficient of the plain flap and the morphing flap at AoA=0deg

Regarding the surface streamlines it can be seen that for the moderate angle of attack of AoA = 0deg the flow is almost completely attached to the HWB components. Both the plain flap and the morphing flap are detached in the landing configuration in accordance with the results of the design studies, whereas the flow on both flaps is completely attached again in the take-off position and the resulting low flap deflection angle. It is also noticeable that there is still a positive pressure gradient in the region of the optimized center body below the engine, which will be analyzed in more detail at higher angles of attack in upcoming studies. In the course of this, analyzes of the flow on the T-tail, the nacelle and especially at the nacelle's inlet are also examined in more detail.

6. CONCLUSION

In the course of the SIAM project a hybrid wing body was developed by Iwanizki et al. from the perspective of noise reduction in accordance with "Flightpath 2050". Noise-reducing aspects such as noise shielding and gapless high-lift systems were already considered in the preliminary design. Building on the preliminary design, the detailed engine integration and the detailed wing design including a high-lift system were carried out. The engine integration was largely driven by noise reduction and controllability of the aircraft, which predefines the position of the engine. The final engine installation is a noise shielding effectively podded engine design at a streamwise position at 63 % of the center body length with an achieved drag reduction of ΔC_D = -0.0107 compared to the center body with unadapted integration.

Comparing the SIAM HWB design with the HWB design from Lockheed Martin [15], it is noticeable that a significant improvement in L/D and fuel consumption can be achieved, especially by positioning the engine further back. Since the SIAM HWB design is acoustically driven, it is another option to explore buried engines compared to a podded engine design, which could be a more efficient option, because of the benefits of the boundary layer ingestion. However, the cabin design would be challenging here, which still needs to be optimized for the current SIAM HWB.

Based on the preliminary design and engine integration, the cruise and the high-lift wing were designed in several iterations. For the cruise wing, profiles with a high relative thickness were designed inversely, which enable a local lift coefficient of c_l = 0.42 at Ma = 0.78 and at the same time, mitigate the risk of early stall in low-speed compared to the preliminary designed profiles.

The high-lift system was designed within 2D and afterwards 3D studies using RANS simulations. The high-lift system was designed as a gapless plain flap. In addition, a morphing flap was designed, which has no additional noise source at the flap side edges due to a form adaptive gap cover triangle. In addition to the advantages in terms of noise emissions, the plain flaps have the advantage of a comparable light structure without flap-track-fairings. The CFD investigations of the 3D high-lift configuration showed that the targeted lift coefficients of $C_{L,TO}$ = 0.76 and $C_{L,LDG}$ = 0.96 can be achieved by the HWB with the use of the designed conventional plain flap as well as with the morphing flap. The SIAM HWB even has the potential to optimize the planform further since, eg. no leading-edge devices had to be designed for low-speed. With eg. a low-noise smart droop nose, the total C_L of the HWB can be increased even further.

As part of the high-lift design, the aileron was also designed as a plain flap. In the future, the aileron could be designed as a shape-adaptive structure, as for example Wildschek et al. [30] have demonstrated. The entire trailing edge of the wing could be designed to be shape-adaptive. Such a shape adaptive wing can be used for controllability, load reduction and noise reduction due to the absence of gaps. Overall, the SIAM HWB still has considerable potential for further optimizations both in terms of aerodynamic performance and noise reduction.

ACKNOWLEDGEMENT

REFERENCES

[1] European Commission, Directorate-General for Mobility and Transport, Directorate-General for Research and Innovation, Flightpath 2050 : Europe's vision for aviation : maintaining global leadership and

serving society's needs, Publications Office, 2011. doi: 10.2777/50266M.

[2] F. Wienke, L. Bertsch, J. Blinstrub, M. Iwanizki, P. Balack, J. Häßy, System noise assessment of conceptual tube-and-wing and blended-wing-body aircraft designs, AIAA 2023-4170. *AIAA AVIATION 2023 Forum*. June 2023. doi: 10.2514/6.2023-4170

[3] M. Iwanizki, D. Keller, F. N. Schmidt, Y. J. Hasan, J. Kurz, F. Wienke, L. Bertsch, M. Mößner, P. Balack, J. Häßy, B. Fröhler, Conceptual Aircraft Design Activities Related to Blended Wing Body Configurations in the Scope of the DLR Project SIAM. EUCASS-3AF 2022, 27. Jun. - 01. Jul. 2022, Lille, France, 2022. doi: 10.13009/EUCASS2022-6104.

[4] J. Hooker, Design of a Hybrid Wing Body for Fuel Efficient Air Mobility Operations at Transonic Flight Conditions, AIAA 2014-1285. 52nd Aerospace Sciences Meeting. January 2014. doi: 10.2514/6.2014-1285

[5] P. Okonkwo, H. Smith, Review of evolving trends in blended wing body aircraft design, Progress in Aerospace Sciences, Volume 82, 2016, Pages 1-23, ISSN 0376-0421.doi: 10.1016/j.paerosci.2015.12.002

[6] Z. Spakovszky, Advanced low-noise aircraft configurations and their assessment: past, present, and future, CEAS Aeron. Journal 10.1, 2019, 137-157

[7] R. Thomas, C. Burley, C. Nickol, Assessment of the noise reduction potential of advanced subsonic transport concepts for NASA's Environmentally Responsible Aviation Project. In 54th AIAA Aerospace Sciences Meeting, 2016, p. 0863.

[8] R. Liebeck, Design of the blended wing body subsonic transport. J. of aircraft, 2004, 41(1), 10-25

[9] J. Hileman, Z. Spakovszky, M. Drela, M. Sargeant. Aerodynamic and Aeroacoustic Three-Dimensional Design for a "Silent" Aircraft, AIAA 2006-241. 44th AIAA Aerospace Sciences Meeting and Exhibit. January 2006. doi: 10.2514/6.2006-241

[10] J. Delfs, *Airframe Noise.* In: Aircraft Noise VKI Lecture Series, 2012. Von Karman Institute for Fluid Mechanics, Brussels. Seiten 1-54. ISBN 13 978-2-87516-029-4.

[11] W: Dobrzynski, B. Gehlhar, H. Buchholz, Model- and full scale high-lift wing wind tunnel experiments dedicated to airframe noise reduction. Aerospace Science and Technology, 2001, 5:27–33

[12] L. Enghardt, L. Design of Low Noise UHBR Engines. SFB 880 Forschungsklausur, 20.09. - 21.09.2016, Bremen, Germany, 2016.

[13] W Dalton, Ultra High Bypass Ratio Low Noise Engine Study, 2003, NASA/CR 003-212523

[14] J. Hooker, Design of a Hybrid Wing Body for Fuel Efficient Air Mobility Operations at Transonic Flight Conditions, AIAA 2014-1285. 52nd Aerospace Sciences Meeting. Jan.2014.doi:10.2514/6.2014-1285

[15] J. Hooker, A. Wick, C. Hardin, Commercial Cargo Derivative Study of the Advanced Hybrid Wing Body Configuration with Over-Wing Engine Nacelles, 2017, NASA CR 2017-219653

[16] D. Chan, J. Hooker, A. Wick, R. Plumley, C. Zeune, M. Ol, J. DeMoss, Transonic Semispan Aerodynamic Testing of the Hybrid Wing Body with Over Wing Nacelles in the National Transonic Facility, AIAA 2017-0098. 55th AIAA Aerospace Sciences Meeting. January 2017. doi: 10.2514/6.2017-0098

[17] John R. Hooker, Andrew Wick, Cale H. Zeune and Anthony Agelastos. "Over Wing Nacelle Installations for Improved Energy Efficiency," AIAA 2013-2920. 31st AIAA Applied Aerodynamics Conference. June 2013. doi: 10.2514/6.2013-2920

[18] Z. Xin, Z. Chen, W. Gu, G. Wang, Z. Tan, D. Li, B. Zhang, Nacelle-airframe integration design method for blended-wing-body transport with podded engines, Chinese Journal of Aeronautics, Volume 32, Issue 8, 2019, Pages 1860-1868, ISSN 1000-9361. doi:10.1016/j.cja.2019.06.009

[19] D. Keller, Aerodynamic Investigation of Propulsion Integration for a Low Noise Hybrid Wing-Body with Podded UHBR Turbofan Engines. 13th EASN International Conference, Sept. 2023, Salerno, Italy.

[20] M. Hepperle, Braunschweig Germany, 2005. https://www.dlr.de/as/Portaldata/5/Resources/dokumente/projekte/vela/The_VELA_Project.pdf. Retrieved on: 06.09.2023

[21] D. Schwamborn, T. Gerhold, R. Kessler, DLR-TAU code - an overview, In 1st ONERA/DLR Aerospace Symposium, Paris, 21.-24. Juni 1999, pages S4–2–S4–10, 1999.

[22] T. Streit, N. Hofrogge, DLR transonic inverse design code, extensions and modifications to increase versatility and robustness. In: RAeS 2016 Appllied Aerodynamics Conference, Bristol, 2016.

[23] R. Eppler, Airfoil design and data, Springer Verlag GmbH, Heidelberg, 1990.

[24] M. Fink, D. Bailey, Model tests of airframe noise reduction concepts. 6th Aeroacoustics Conference 04 June 1980 - 06 June 1980 Hartford, CT, USA.

[25] S. Kota, P. Flick, F. Collier, Flight Testing of FlexFloilTM Adaptive Compliant Trailing Edge, AIAA 2016-0036. 54th AIAA Aerospace Sciences Meeting. January 2016. doi: 10.2514/6.2016-0036

[26] DLR German Aerospace Center, „Research into flexible wing surfaces at DLR", Braunschweig, Germany, June, 2020 https://www.dlr.de/en/latest/news/2020/02/20200604_dlr-research-into-flexible-wing. Retrieved on: 01.09.2023

[27] D. Paulus, S. Binder, Ö. Petersson, H. Baier, M. Hornung, The Integration of an Efficient High Lift System in the Design Process of a Blended Wing Body Aircraft, AIAA 2012-5650. 12th AIAA Aviation Technology, Integration, and Operations (ATIO) Conference and 14th AIAA/ISSMO Multidisciplinary Analysis and Optimization Conference. September 2012. doi: 10.2514/6.2012-5650

[28] M. Spearman, Wind-Tunnel Investigation of an NACA 009 Airfoil with 0.25- and 0.50-Airfoil-Chord Plain Flaps Tested Independently and in Combination, 1948, NACA TR 1517

[29] M. Radestock, J. Riemenschneider, A. Falken, J. Achleitner, Experimental Study of Flexible Skin Designs Between a Moving Wing Segment and a Fixed Wing Part on a Full Scale Demonstrator, Proceedings of the ASME 2020 Conference on Smart Materials, Adaptive Structures and Intelligent Systems SMASIS2020, September 14-16, 2020, Irvine, CA, USA. doi: 10.1115/SMASIS2020-2310

[30] A. Wildschek, T. Havar, K. Plötner, An all-composite, all-electric, morphing trailing edge device for flight control on a blended-wing-body airliner, Journal of Aerospace Engineering, 2009, 224(1), pp: 1 - 9. doi: 10.1243/09544100JAERO622